RSC Advances

This article can be cited before page numbers have been issued, to do this please use: Y. Shen, Y. Liu, W. Wang, F. Xu, C. Yan, J. Zhang, J. Wang and A. Yuan, *RSC Adv.*, 2016, DOI: 10.1039/C6RA05225H.

ROYAL SOCIETY OF CHEMISTRY

www.rsc.org/advances

View Article Online
DOI: 10.1039/C6RA05225H

Journal Name

ARTICLE

Au Nanocluster Arrays on Self-assembled Block Copolymer Thin Films as Highly Active SERS Substrates with Excellent Re-producibility

Received 00th January 20xx,
Accepted 00th January 20xx

DOI: 10.1039/x0xx00000x

www.rsc.org/

Yale Shen, [a] Yuanjun Liu,[a,*] Wei Wang,[b] Fan Xu,[b] Chao Yan,[b] Junhao Zhang,[a] Jing Wang,[a] Aihua Yuan[a,*]

We demonstrate the fabrication of uniform Au nanocluster arrays utilizing self-assembled polystyrene-*block*-poly(4-vinylpyridine) (PS-*b*-P4VP) thin film as template and their application as surface-enhanced Raman scattering (SERS) substrate. Au nanocluster arrays were fabricated by *in situ* heating and UV light-assisted reduction of Au precursor ($AuCl_4^-$) which has been selectively loaded on the surface of PS-*b*-P4VP thin film. It was found that the formation of Au particles involves two steps, the *in situ* reduction of $AuCl_4^-$ forming tiny Au particles and the fusion of tiny Au particles forming bigger Au particles. The Au particle density and size are tunable by adjusting the temperature and time of UV light assisted reaction step. Uniform and high density Au nanocluster arrays are formed at 80 °C with three hours. The arrays were then used as SERS substrate for detecting a model molecular (R6G), which shows an excellent SERS performance with high reproducibility. The signals collected at 120 points over a 50 μm × 50 μm area give relative standard deviation lower than 11 %. These results indicate that the route provides a simple, low-cost, environmental, and reproducible method for fabricating high-active SERS substrates.

Introduction

Surface enhanced Raman spectroscopy (SERS) is an ultrasensitive molecular spectroscopic technique, which can provide vibrational signatures to detect and identify molecules on or near the surface of plasmonic nanostructures.[1-4] SERS has recently been applied in various detection fields, such as environmental monitoring, pesticide residue analysis, disease markers, food safety control, and other chemical and biological applications.[5-11] There are two mechanisms, chemical enhancement (CM) and electromagnetic enhancement (EM), widely accepted to account for SERS.[12] The electromagnetic enhancement is related to surface plasmon polariton resonance occurring in the nanogaps between nanoparticles (known as "hot spots"), which induce strong electromagnetic field enhancement and thus strong SERS-active signals.[2, 13, 14]

For improving SERS performance, the substrate is the first focus, which directly influences the density of "hot spots". Noble metal nanoparticles such as gold and silver with characteristic optical properties due to localized surface plasmon resonance (LSPR) [9, 15] have been widely used for generating "hot spots" on SERS substrates. It has been demonstrated that a suitable SERS substrate should possess not only abundant and uniform "hot spots" but also a large surface area to absorb plenty of analyte molecules.[16-18] The SERS substrate with periodic array-like microstructure is highly preferred due to its high uniform "hot spots" distribution and its excellent signal reproducibility. As for Au-based substrate, many different Au nanoarrays have been designed and prepared for SERS substrate. The reported Au nanoarrays include Au nanoantenna arrays prepared by colloid assembled template,[19] Au nanopillar arrays prepared by nanoimprinting transfer route,[20] Au nanocuboid periodic substrate prepared through E-beam lithography,[21] plasmonic Au nanogalaxies prepared through E-beam lithography and chemical reduction,[22] and so on. Among various array-like substrate, nanoparticle cluster arrays[23] are a novel class of engineered substrates for SERS, in which the nanoparticles interact on multiple length scales to create a multiscale E-field cascade enhancement. However, few reports are about Au nanoparticle based cluster arrays for SERS substrate, partially owing to the difficulty of Au cluster arrays preparation. Recently, Yang *et al*[24] obtained Au nanoparticle cluster arrays by E-beam lithography and the following particle binding deposition technique. Although lithography technique can fabricate well-controlled nanoarrays with high enhancement factor and excellent reproducibility, it is limited by the high cost, the preparation speed, and the difficult to be extended to large areas.[25]

In this work, we demonstrate a simple, inexpensive and environmental route to fabricate a high SERS-active substrate composed of uniform Au nanocluster arrays. With the self-

[a] School of Environmental and Chemical Engineering, Jiangsu University of Science and Technology, Zhenjiang 212003, P. R. China. Email: liuyuanjun@just.edu.cn; aihua.yuan@just.edu.cn; Tel: +86 0511-85639001
[b] School of Material Science and Engineering, Jiangsu University of Science and Technology, Zhenjiang 212003, P. R. China.

View Article Online
DOI: 10.1039/C6RA05225H

Journal Name

ARTICLE

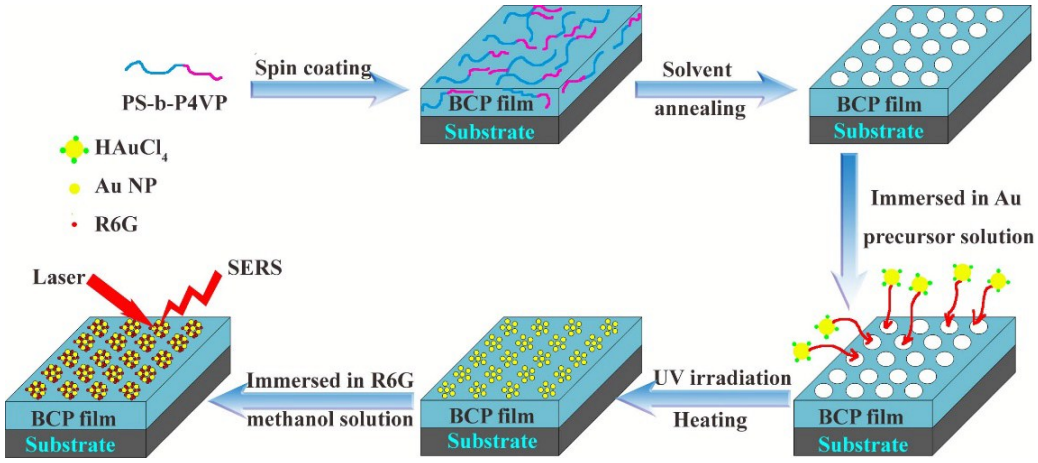

Scheme 1. Schematic illustration for the preparation of Au nanocluster arrays.

assembled amphiphilic diblock copolymer as template, Au precursor was firstly loaded on the P4VP region of the amphiphilic diblock copolymer polystyrene-*block*-poly(4-vinylpyridine) thin film. The following UV light assisted *in situ* reduction at different temperature induces the formation of cluster-like Au nanoarrays. The composite arrays were then investigated as SERS substrate. It was found that the obtained substrate shows excellent SERS performance with SERS enhancement factor up to 1.7 $\times 10^6$. Especially, the cluster-like array show good reproducibility. The SERS signals show quite small relative standard deviation (< 11%), suggesting the high reliability and favourable stability of the obtained SERS substrate.

Results and discussion

Gold cluster-like arrays were fabricated with the assistance of PS-*b*-P4VP self-assembled nanopatterns. Scheme 1 illustrates the fabrication procedure. PS-*b*-P4VP diblock copolymer thin films were firstly prepared by spin-coating PS-*b*-P4VP solution onto the silicon substrates. The film was then annealed in 1, 4-dioxane vapour inducing the formation of ordered arrays, vertical P4VP nanocylinder arrays enclosed by PS matrix. The array-like PS-*b*-P4VP thin films were then immersed in $HAuCl_4$ solution. In the acidic solution, the pyridinic nitrogen in P4VP block is protonated, which will selectively attract negative $AuCl_4^-$ complexes due to the electrostatic interaction.[26-29] After that, the $AuCl_4^-$ loaded PS-*b*-P4VP thin film was irradiated under UV light at suitable temperature. Metallic gold were *in situ* generated on the film forming ordered Au nanocluster arrays. Photochemical reduction is a useful, green route to transfer $AuCl_4^-$ complexes to Au nanoparticles. No any solvent or strong reducing agent was needed in the reduction process. Especially, the thus obtained Au particles often have clean surface.

The corresponding cross-sectional SEM image (shown in Fig. SI-1, see Supporting Information) indicates that some cylindrical microdomains are oriented vertically on the substrate. The thickness of the film was determined to be about 230 nm. Fig. 1a presents atomic force microscope (AFM) height image of the as-annealed PS-*b*-P4VP thin film, which also clearly shows vertically oriented nanocylinder arrays. We noted that the AFM image measured in the phase mode (Fig. 1b) shows the harder material, the P4VP blocks as brighter colour, while the PS matrix is dark.[30] Hence the cylindrical domains are composed by P4VP blocks, and the surrounded matrix is composed by PS domain. The average diameter of the cylindrical nanodomains is 43 nm, while the average center to center distance between the adjacent cylindrical domains is 57 nm. The density of the nanocylinders is about 1.75×10^{10} cm^{-2}.

Fig. 1c gives the transmission electron microscopy (TEM) image of Au nanocluster array fabricated on the highly ordered PS-*b*-P4VP template. Exposing the $AuCl_4^-$ loaded PS-*b*-P4VP thin film to UV irradiation induces the reduction of Au(III). The formed Au nanoparticles are *in situ* deposited on the film. It was found that the Au nanoparticles are distributed on the film with cluster-like shape. The Au nanoclusters with size of ~51 nm are nearly hexagonally arrayed. This size is a little bigger than that of original P4VP nanodomains. Interestingly, each Au cluster is further composed of several tens of tiny Au nanoparticles. These tiny nanoparticles have size in the range of

View Article Online
DOI: 10.1039/C6RA05225H

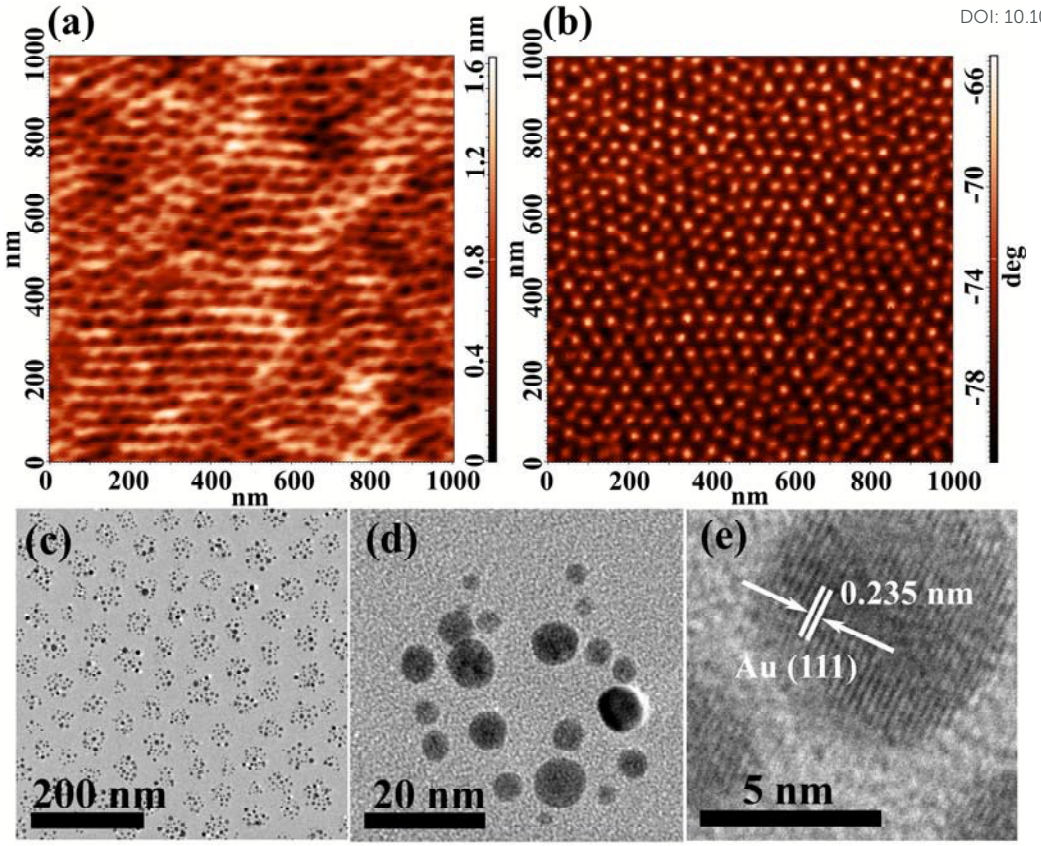

Fig. 1 AFM height (a) and phase (b) images of self-assembled PS-*b*-P4VP thin film, the scanning size of both images is 1.5×1.5 μm^2. TEM or HRTEM images of (c) Au naonocluster arrays, (d) Au nanocluster, (e) Au nanoparticle prepared at 80 °C with 3 h.

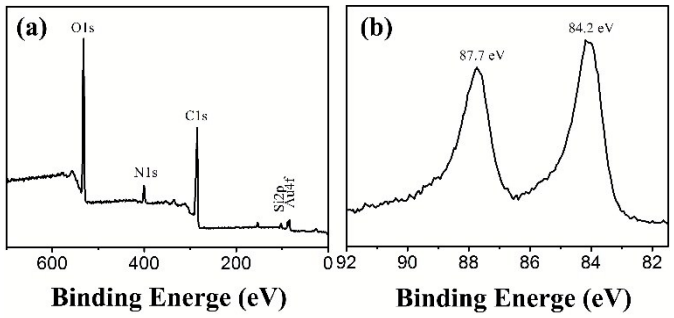

Fig. 2 (a) XPS spectrum of Au nanocluster array. (b) The high-resolution XPS spectrum of Au 4f.

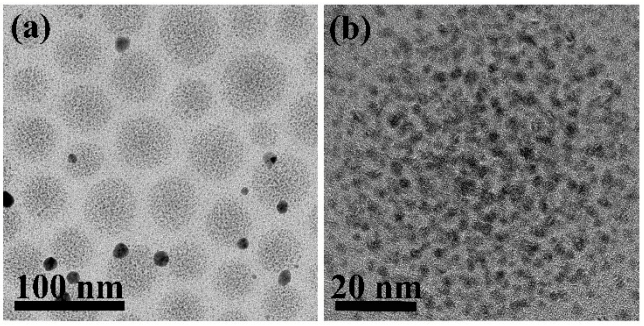

Fig. 3 (a) TEM image of the Au nanocluster array thin film prepared at 80 ° C with 1 h, (b) the corresponding magnified TEM image of the Au cluster.

3-10 nm (Fig. 1d). Fig. 1e shows the high-resolution TEM (HRTEM) image of a Au nanoparticle. The observed lattice spacing of 0.235 nm can be corresponded to (111) crystal plane of cubic Au.[31]

X-ray photoelectron spectroscopy (XPS) measurement was then performed to further study the composition and oxidation state of Au nanocluster arrays. The XPS spectrum of Au nanocluster arrays (Fig. 2a) shows elements of Au, C, N, and Si in the sample. Among them, Si and O are the mainly elements of quartz substrate, while the elements, C and N, come from the PS-*b*-P4VP film. Fig. 2b demonstrates the high-resolution XPS spectrum of Au. The Au 4f $_{7/2}$ and Au 4f $_{5/2}$ peaks locate at binding energies of 84.2 eV and 88.7 eV, which are the typical values for metallic Au.[32] To investigate the formation process of the cluster-like Au arrays, a contrast experiment with shorter irradiation time (1 h) was carried out while keeping other experimental parameters constant. Fig. 3 shows the corresponding Au nanocluster arrays obtained with 1 h of irradiation. It can be seen that with 1 h of irradiation at 80 ^{o}C, uniform circular cluster array was formed (Fig. 3a). Fig. 3b shows a magnified TEM image of one Au nanocluster. The Au nanocluster is composed of numerous 2 nm of Au particles, which are highly selectively loaded on the P4VP domain. This shows that with the increasing of irradiation time, relatively bigger primary Au nanoparticles (3-10 nm) will form. In contrast, the particle number in one cluster decreases with increasing irradiation time. Hence, it is proposed that the photochemical reduction process involves two steps, the

View Article Online
DOI: 10.1039/C6RA05225H

Journal Name

ARTICLE

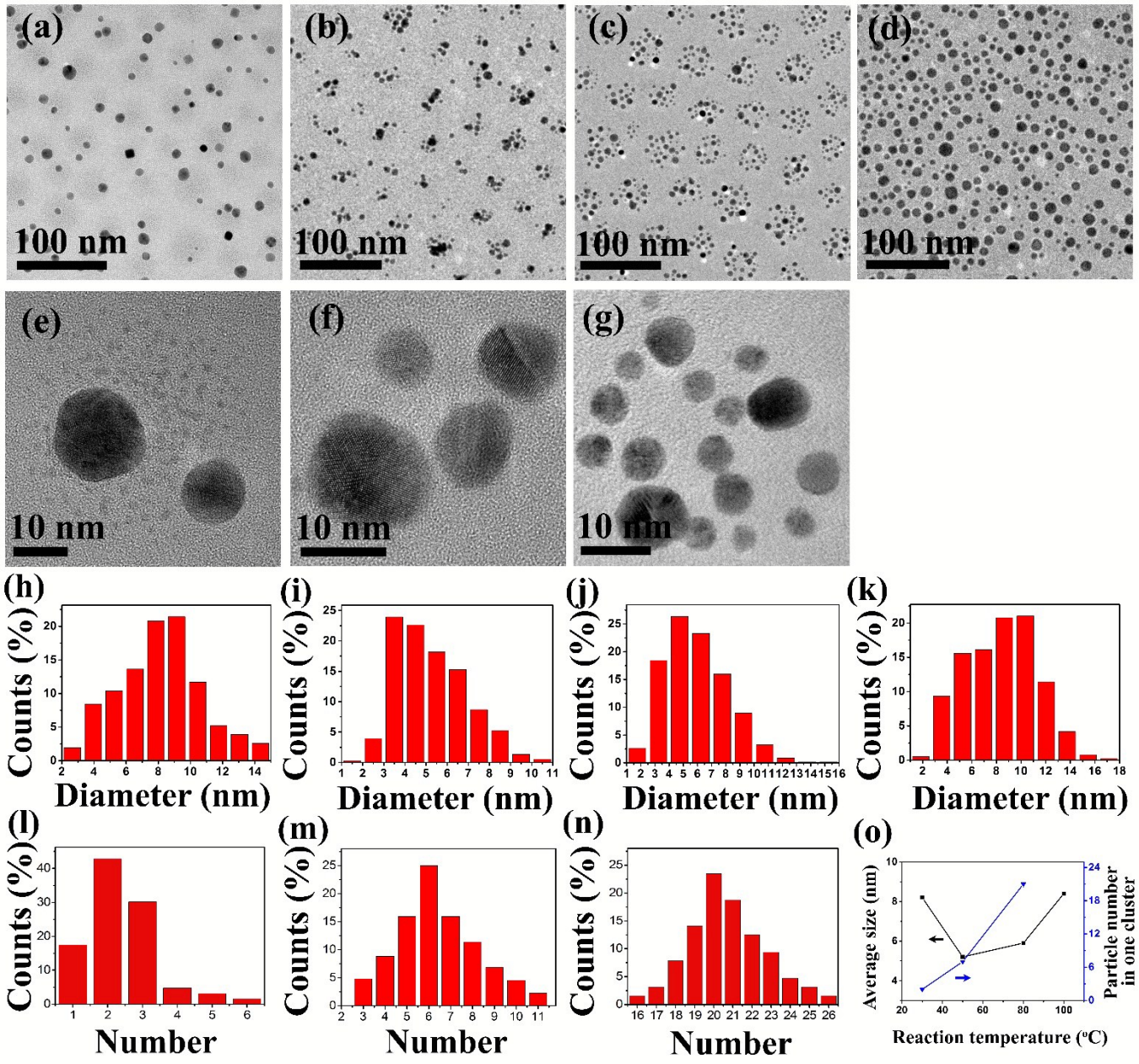

Fig. 4 TEM images of the Au nanocluster array prepared for 3 h with different reduction temperatures. (a) 30 °C, (b) 50 °C, (c) 80 °C, and (d) 100 °C. (e), (f), and (g) are the magnified single cluster corresponding to figure (a), (b), and (c), respectively. (h), (i), (j), and (k) demonstrates size distributions of bigger Au particles in the clusters corresponding to (a), (b), (c), and (d), respectively. (l), (m), and (n) show the Au particle number with bigger size in one cluster corresponding to figure (a), (b), and (c), respectively. (o) The relationship between the reaction temperature and average size or particle number of bigger Au particles in one cluster.

reduction of Au (III) to Au and the aggregation/fusion of smaller Au particles to form relatively bigger Au particles.

Controlled experiments with different reduction temperatures were also performed. It was found that the temperature also plays an important role on the reduction of $AuCl_4^-$. Fig. 4a shows the TEM image of the product obtained with 30 °C. Cluster-like array was observed with this temperature (Fig. 4a). Fig. 4e demonstrated a single Au cluster.

The Au cluster formed at this temperature contains mainly 1-3 bigger Au nanoparticles with size of 6-12 nm and about one hundred of tiny Au nanoparticleswith size of ~2 nm (Fig. 4e, 4l). This would relate to the formation mechanism, that is, the formation of relatively small Au nanocrystals firstly and then the fusion of them forming relatively bigger Au nanoparticles (the detailed mechanism will be discussed in the following text). Fig. 4b shows TEM image of the nanocluster array obtained with reduction temperature of 50 °C. Most clusters contain 3-7 bigger Au particles with size of 3-7 nm in one cluster. It should be noted that many tiny nanoparticles with smaller sizes are also observed in the background. With reaction temperature of 80 °C, high-density Au nanocluster arrays were obtained (Fig. 4c). The particle number in one cluster increases to be about 20 (Fig. 4n). For this sample, few tiny Au nanoparticles with size < 2 nm were observed during TEM observation. While, further increasing the temperature to 100 °C, Au nanoparticles instead of cluster-like structure randomly disperse on the surface of the PS-*b*-P4VP thin film (Fig. 4d). It seems that these Au nanoparticles with bigger size were not confined within the P4VP nanodomains. Fig. 4l-n shows the statistical result of Au particle number with bigger size in one cluster. Obviously, with the increasing of reduction temperature, the average bigger particle number in one cluster gradually increases from 2 to about 20 (Fig. 4o). The histograms of Fig. 4h-k illustrate that the size distribution. The average diameters of the bigger Au nanoparticles obtained at different temperatures are 8.2 nm, 5.2 nm, 5.9 nm, and 8.4 nm for 30 °C, 50 °C, 80 °C, 100 °C, indicating a complex size change trend with increasing reduction temperature (Fig. 4o). These results suggest that a suitable temperature is critical for the formation of cluster-like arrays.

From the above experiments, the formation process of Au cluster-like array is proposed as follows. During the immersing step, $AuCl_4^-$ ions were selectively coordinated with P4VP domains on the thin film. Upon UV light irradiation, $AuCl_4^-$ ions coordinated on P4VP domains were reduced to Au, forming cluster-like arrays. The involved chemical reactions can be described as follows:[33]

$$2Au^{III}Cl_4^- \rightarrow 2Au^{II}Cl_3^- + Cl_2,$$
$$2Au^{II}Cl_3^- \rightarrow Au^{I}Cl_2^- + Au^{III}Cl_4^-,$$
$$2Au^{I}Cl_2^- \rightarrow Au^{II}Cl_3^- + Au^0 + Cl^-.$$

Owing to the anchoring of P4VP domain to $AuCl_4^-$ ions, the *in situ* formed metallic Au locates on the P4VP region forming cluster-like arrays. The newly formed metallic Au has smaller size of ~2 nm. During the following ripening step, the adjacent tiny Au particles will break the anchoring of P4VP, diffuse, and then fuse together forming Au nanoparticles with bigger size driven by the decrease of surface energy and thermal vibration. The diffusion-fusing process would be temperature dependent. At relatively lower temperature (such as 50 °C), the Au diffusion-fusing trend would be low, only minority of them was fused. Hence the cluster composes only 3-7 Au particles. While majority of tiny Au particles exist as the form of tiny Au particles with size of ~2 nm. With higher temperature such as 100 °C, the diffusion-fusing process would be quite strong. Most Au particles would break the anchoring of P4VP region. The formed bigger Au particles randomly deposite on the film without array-like structures. It should be noted that the Au particle size (bigger Au particle size) not only depends on the number of fused tiny Au particles but also on the fusion site number (the number of bigger Au particle in one cluster). At lower temperature such as 30 °C, although less tiny Au particles fused, the fusion site is also less, so relatively more Au tiny particles would fuse into one bigger Au particle. This causes an abnormal bigger Au size formed at 30 °C (Fig. 4o).

Uniform noble metal nanoparticles array could deliver excellent SERS performance. It is proposed that the separation distance between nanoparticles in the range of 5-100 nm and the nanoparticle size of 20-70 nm is quite favorable for the SERS performance.[34, 35] There are also reports that highly ordered Au particle arrays with separation distance between nanoparticles down to <5 nm also exhibit excellent SERS performance.[36] Thus, it is believed that our prepared cluster-like Au arrays on PS-*b*-P4VP thin film would have numerous "hot spots", which could observably extend Raman intensity of the analytes. In addition, our Au nanocluster arrays were formed on silicon substrate with weak Raman signals, which have little interference on the investigation of SERS performance.

In order to evaluate the SERS detection performance of the prepared cluster-like Au array substrate, Rhodamine 6G (R6G) was selected as model molecule. The Au cluster arrays formed at different temperature were firstly investigated as the cluster parameter and Au nanoparticle size were tuned obviously. Figure 5a shows the SERS spectra of 10^{-5} M R6G methanol solution collected with cluster-like Au arrays prepared at different temperatures. It can be clearly seen that the Au arrays formed at 80 °C shows the strongest Raman signals, suggesting the best SERS performance. The enhancement factor (EF) was calculated to quantitatively demonstrate the SERS performance. With the peak at 1648 cm^{-1}, EF was calculated by the formula:[37]

$$EF = \frac{I_{SERS}N_0}{I_0N_{SERS}} = \frac{I_{SERS}n_0N_A}{I_0n_{SERS}N_A} = \frac{I_{SERS}C_0V_0}{I_0C_{SERS}V_{SERS}} = \frac{I_{SERS}C_0}{I_0C_{SERS}}$$

where N_0 and I_0 are the number of molecules and intensity of regular Raman measurement with 0.01 M R6G solution, N_{SERS} and I_{SERS} are those of SERS measurement with the same solution. From this formula, EF values were calculated based on the peak at 1648 cm^{-1}. The substrates prepared at 30 °C, 50 °C, 80 °C, 100 °C provide EF values of 1.3×10^6, 1.4×10^6, 1.7×10^6 and 0.6×10^6, respectively. It shows that with the increasing of reaction temperature from 30-80 °C, the EF correspondingly increases.

With the increasing of reaction temperature from 30 to 80 °C, the tiny Au particles in the cluster gradually fused into bigger Au particles with size of 3-8 nm. The density of bigger Au particles on the film correspondingly increases. The EF also gradually increases. This indicates that the SERS performance was mainly contributed by the bigger Au particles. The increased density of bigger Au nanoparticles is expected to translate into a high density of "hot spots" for SERS, particularly when the clusters are uniform and highly ordered such as that of our prepared Au arrays formed at 80 °C. In

View Article Online
DOI: 10.1039/C6RA05235H

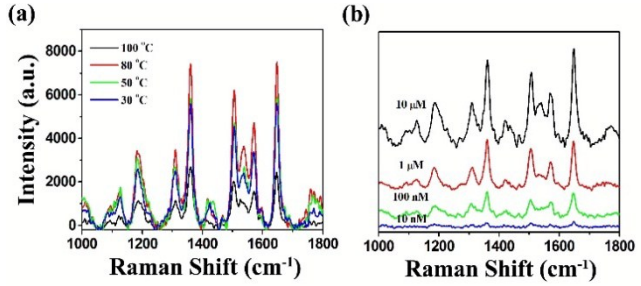

Fig. 5 (a) SERS spectra of 10^{-5} M R6G methanol solution collected by the Au cluster-like array films prepared at different temperatures. (b) SERS spectra of Au cluster-like array films (prepared at 80 °C) immersed in different concentration of R6G methanol solutions.

addition, the Raman signal enhancement by the Au cluster arrays was also compared against unpatterned Au nanoparticle thin film (obtained at 100 °C), which validated the better performance of the cluster-like Au arrays (Fig. 5a).

It was reported that the metal nanocluster composed of many tiny particles would become a single metal particle with proper treatment process. We then tried to transform the Au nanoclusters (shown in Figure 1) to single particles by heating the film at 200 °C in N_2 atmosphere for 30 min. After that, the film was characterized by TEM. As shown in Fig. SI-2, the cluster structure disappeared, while single Au nanoparticles with size of 17-26 nm formed on the film. However, the array-like structure is also broken, suggesting that during the heating process, the Au particles would break the anchoring of P4VP forming non-array-like particle film. The SERS performance of the corresponding Au film was then investigated with similar method (Fig. SI-3), which gives EF of 7.2×10^4. This value is much lower than that of Au nanocluster array (with EF of 1.3-1.7×10^6).

In addition, we also prepared another substrate through simple spherical micelle for comparison (see experimental section). The obtained film also shows cluster-like structure composed of Au nanoparticles with size of ~8 nm and cluster size of 42 nm (Fig. SI-4). The SERS performance of the substrate is shown in Fig. SI-5. Clearly, the substrate prepared with spherical micelle (with EF of 4.3×10^5) also shows relatively weak SERS performance than that prepared with cylinder-like film (Figure 1, EF of 1.7×10^6). These comparison studies suggest that the better SERS performance of Au nanocluster array film would be contributed by the cluster-like array structure.

To evaluate the detection sensitivity of the Au nanocluster arrays film, SERS spectra of the thin film (prepared at 80 °C) immersed in different concentrations of R6G methanol solution (from 10 μM to 10 nM) were measured. With 10 nM of R6G methanol solution, the Raman characteristic peaks of R6G are even displayed clearly (Fig. 5b). This proved that the SERS substrate could detect very small amount of R6G in which the concentration was even down to 10 nM.

To further semi-quantitatively assess the uniformity of these SERS signals, we investigated 120 spots for SERS mapping-scan spectra. The Raman mapping was scanned over a 50 ×50 μm^2 area with a step size of 5 μm. Figure 6a shows the Raman intensity mapping figure of R6G on the cluster-like Au arrays. The SERS effect is reliable and applicable. The relative standard deviations (RSD) of the Raman intensity for different Raman peaks were also calculated. The RSD values for vibrations at 1310, 1361, 1510, and 1648 cm^{-1} (Fig. 6c-f) are 11.28%, 8.37%, 9.28%, and 8.67%, respectively. This demonstrates that the as-prepared substrate has high uniformity. Less than 11% of the RSD values for the four peaks' further assure the uniform SERS effect, indicating the reproducibility of the as-prepared substrate.[38]

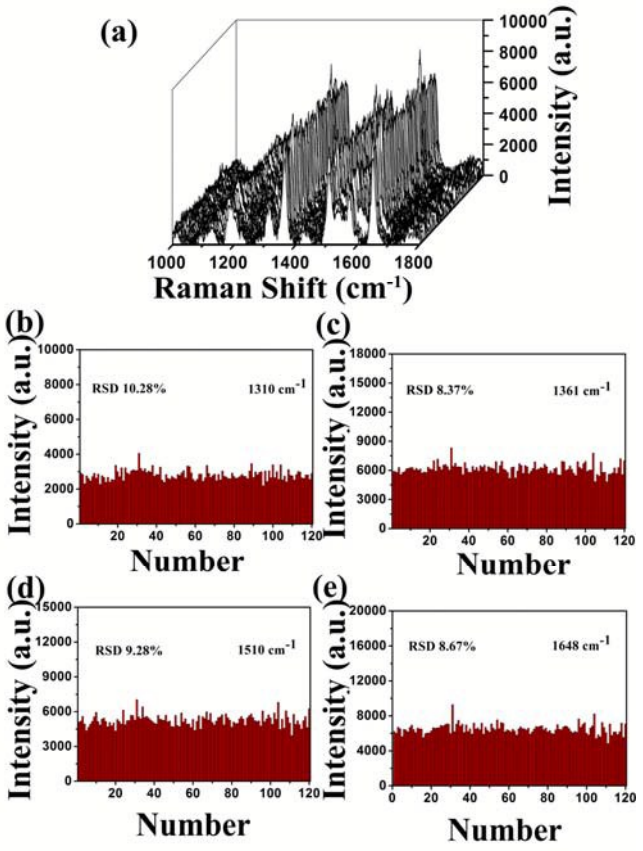

Fig. 6 (a) Raman scattering spectra of 10^{-5} M R6G measured by 120 points over a 50 ×50 μm^2 area with a step size of 5 μm. (b-e) The intensities of the main Raman vibrations of R6G aqueous solution in SERS spectra showed in (a). A 532 nm excitation laser was used.

Experimental

Materials.

Amphiphilic diblock copolymer, polystyrene-*block*-poly (4-vinylpyridine) (PS-*b*-P4VP, Mn = 48000 kg/mol for PS and 25000 kg/mol for P4VP) was purchased from Polymer Source, Inc. Tetrachloroauric (III) acid trihydrate ($HAuCl_4{\cdot}3H_2O$), trichloromethane, 1, 4-dioxane were purchased from Sinopharm Chemical Reagent Co., Ltd. Rhodamine 6G (R6G) was purchased from Sigma-Aldrich.

Preparation of self-assembled PS-*b*-P4VP nanopatterns.

Silica or silicon wafers (1 × 1 cm^2) were firstly immersed in an acidic mixture of 98% H_2SO_4 and 30% H_2O_2 (with volume ratio

of 7:3) with ultrasonic cleaning for 30 min and were strongly rinsed with deionized water for several times. The clean wafers were then dried with the assistance of nitrogen flow. PS-*b*-P4VP was dissolved in trichloromethane to produce a 1 wt% solution. About 20 μL of the PS-*b*-P4VP solution was spin-cast on the clean silicon substrates with 2500 rpm for 40 s to form a film. To induce highly oriented cylindrical P4VP nanodomains in PS matrix, the prepared film was solvent-annealed in a glass vessel (with volume of 27 cm^3). 100 μL of 1, 4-dioxane was added in the vessel as annealing solvent. Then, the vessel was sealed with a stopper and placed at 25 °C for 8 h for solvent annealing. With this process, PS-*b*-P4VP thin film with perpendicularly ordered nanocylinder domains was developed.

Preparation of the Au cluster-like Nanoarrays.

Firstly, $HAuCl_4 \cdot 3H_2O$ was dissolved in the mixture solution of water and ethanol (with volume ratio of = 1:1) with concentration of 24 mM. A drop of the $HAuCl_4$ solution was then dripped onto the PS-*b*-P4VP diblock copolymer film surface and aged for 30 min. After that, the $HAuCl_4$-loaded film was rinsed with deionized water for several times to remove excrescent metal ions and was then naturally dried at room temperature. Subsequent irradiation under UV light (8 W mercury lamp) at 80 °C for 3 h induces the reduction of $HAuCl_4$ to Au nanoparticles, forming Au cluster-like arrays. For investigating the influence of experiment parameters on the structure of Au cluster-like nanoarrays, a series of experiments were carried out with different reaction time (1 h) or temperatures (30 °C, 50 °C, 100 °C) but keeping other conditions constant.

For comparison, a contrast SERS substrate was prepared through simple spherical micelle. 100 μL of 0.024 mol/L $HAuCl_4$ solution were firstly dispersed into 1 mL of PS-b-P4VP solution with concentration of 10 mg/mL by strong stirring, forming spherical micelle. 20 μL of the obtained mixture (spherical micelle) was then spin-coated on a silicon substrate to form a film. Without solvent annealing treatment, the film was then UV-irradiated at 80 °C for 3 h to transfer of Au (III) to metallic Au. The obtained film also shows cluster-like structure (as shown in Fig. SI-4) composed of Au nanoparticles.

Surface-Enhanced Raman Scattering analysis.

The Au nanocluster arrays on the silicon wafers were then used as SERS substrates. To detect SERS enhancement factor, SERS sample was prepared as follows: the SERS substrate was firstly soaked in 0.5 mL of R6G methanol solution to absorb R6G molecules for 30 min, followed by the evaporation of methanol solvent. A 532 nm laser with power of 0.2 mW was then used for Raman scattering analysis. The accumulation time was set as 1 s. We randomly measured 15 different points on the same SERS substrate and averaged them to obtain reliable Raman scattering spectrum.

Characterization.

The topography of the PS-*b*-P4VP thin films was scanned by an atomic force microscope (AFM) (NTEGRA Probe Nano Laboratory, NT-MDT Co.) working on semi-contact mode with a silicon cantilever (spring constant of 2 N/m and resonance frequency ~98 kHZ) and a Hitachi S-4800 field emission scanning electron microscope (SEM). The Au nanocluster arrays were further characterized by a transmission electron microscope (TEM) (Tecnai G2 F30 S-Twin, FEI, Netherlands). For TEM in-plane view, the Au film was lifted off from the silicon substrate with the assistance of 2 wt% of HF solution. The composite thin film was then carefully collected on an amorphous carbon film coated copper grid for TEM observation. The gold composition was analysed by X-ray photoelectron spectrometer (XPS) (ESCALAB 250Xi, Thermo Fisher Scientific Inc.). Surface-Enhanced Raman Scattering Analysis was performed with a Raman spectrometer (Renishaw in Via, England).

Conclusions

In summary, we demonstrate a facile synthetic route for fabricating a well-ordered SERS substrate, Au nanocluster arrays, through *in situ* photochemical reduction of Au precursor ($AuCl_4^-$) which was selectively loaded on the P4VP region of the verticaly oriented PS-*b*-P4VP thin film. Both the particle density and the Au particle size of the nanocluster arrays can be tuned by changing the reaction temperature and time. The SERS signals collected on the highly ordered Au nanocluster arrays show larger enhancement effect. Especially, the SERS signals show lower RSD value (less than 11 %), demonstrating that the cluster array with high reproducibility is reliable to be used as SERS substrate. This simple fabrication of Au nanocluster arrays may also be extended to other metals, oxides, and sulfides. Even more to the point, the properties of the cluster arrays will also be extended to other relevant applications, such as energy storage devices, photo catalysis solar cells and metal-enhanced fluorescence.

Acknowledgements

The authors are grateful for financial support from the National Natural Science Foundation of China (No. 51203069, 51102117, 21203079), Natural Science Foundation of Jiangsu province (No.BK2012276, BK20141293), Qing Lan Project of Jiangsu Province, the project of the Priority Academic Program Development of Jiangsu Higher Education Institutions.

Notes and references

1 J. F. Li, Y. F. Huang, Y. Ding, Z. L. Yang, S. B. Li, X. S. Zhou, F. R. Fan, W. Zhang, Z. Y. Zhou, D. Y. Wu, B. Ren, Z. L. Wang and Z. Q. Tian, *Nature,* 2010, 464, 392-395.
2 S. M. Nie and S. R. Emery, *Science,* 1997, 275, 1102-1106.
3 N. P. W. Pieczonka and R. F. Aroca, *Chem. Soc. Rev.,* 2008, 37, 946-954.
4 H. Abramczyk, B. P. Beata, *Chem. Rev*. 2013, 113, 5766-5781.
5 H. K. Lee, Y. H. Lee, I. Y. Phang, J. Wei, Y. E. Miao, T. Liu and X. Y. Ling, *Angew. Chem. Int. Ed.,* 2014, 126, 5154-5158
6 P. Simakova, J. Gautier, M. Prochazka, K. Herve-Aubert and I. Chourpa, *J. Phys. Chem. C,* 2014, 118, 7690-7697.

View Article Online
DOI: 10.1039/C6RA05225H

7 H. Im, K. C. Bantz, S. H. Lee, T. W. Johnson, C. L. Haynes and S. H. Oh, *Adv. Mater*., 2013, 25, 2678-2685.
8 H. B. Zhou, D. T. Yang, N. P. Ivleva, N. E. Mircescu, R. Niessner and C. Haisch, *Anal. Chem*., 2014, 86, 1525-1533.
9 K. Lee and J. Irudayaraj, *Small,* 2013, 9, 1106-1115.
10 Y. Wang, X. J. Zhang, P. Gao, Z. B. Shao, X. W. Zhang, Y. Y. Han and J. S. Jie, *ACS Appl. Mater. Interfaces,* 2014, 6, 977-984.
11 L. M. Tong, T. Zhu and Z. F. Liu, *Chem. Soc. Rev.,* 2011, 40, 1296-1304.
12 K. R. Li, M. I. Stockman and D. J. Bergman, *Phys. Rev. Lett.*, 2003, 91, 227402.
13 L. Osinkina, T. Lohmuller, F. Jackel and J. Feldmann, *J. Phys. Chem. C,* 2013, 117, 22198-22202.
14 J. Zhang, H. Liu, Z. Wang and N. Ming, *Adv. Funct. Mater.,* 2007, 17, 3295-3303.
15 L. A. Lane, X. M. Qian, S. M. Nie, *Chem. Rev*., 2015, 115, 10489-10529.
16 F. L.Cristina, P.Lakshminarayana, M. S.Diego, M. T.José, O. Fernando, C. C. Rafael, P. S. Isabel and P. J. Jorge, *ACS Appl. Mater. Interfaces,* 2015, 7, 12530-12538.
17 Q. Fu, Z. B. Zhan, J. X. Dou, X. Z. Zheng, R. Xu, M. H. Wu and Y. Lei, *ACS Appl. Mater. Interfaces,* 2015, 7, 13322-13328.
18 Y. W. Qian, G. W. Meng, Q. Huang, C. H. Zhu, Z. L. Huang, K. X. Sun and B. Chen, *Nanoscale,* 2014, 6, 4781-4788.
19 P. Kühler, M. Weber and T. Lohmüller, *ACS Appl. Mater. Interfaces,* 2014, 6, 8947-8952.
20 S. J. Barcelo, A. Kim, W. Wu and Z. Y. Li, *ACS Nano,* 2012, 6, 6446-6452.
21 G. Das, M. Chirumamilla, A. Toma, A. Gopalakrishnan, R. P. Zaccaria, A. Alabastri, M. Leoncini and E. DiFabrizio, *Sci. Rep.,* 2013, 3, 1792.
22 A. Gopinath, S. V. Boriskina, W. R. Premasiri, L. Ziegler, B. M. Reinhard and L. DalNegro, *Nano Lett.,* 2009, 9, 3922-3929.
23 W. J. Chao, Y. Kim and J. K. Kim, *ACS Nano,* 2012, 6, 249-255.
24 L. L. Yang, B. Yan, W. R. Premasiri, L. D. Ziegler, L. D. Negro and B. M. Reinhard, *Adv. Funct. Mater.,* 2010, 20, 2619-2628.
25 X. Liu, Y. Shao, Y. Tang and K. F. Yao, *Sci. Rep.,* 2014, 4, 5835.
26 S. K. Cha, J. H. Mun, T. Chang, S. Y. Kim, J. Y. Kim, H. M. Jin and S. O. Kim, *ACS Nano,* 2015, 9, 5536-5543.
27 N. L. Wu, X. Zhang, J. N. Murphy, J. Chai, K. D. Harris and J. M. Buriak, *Nano Lett.,* 2012, 12, 264-268.
28 D. O. Shin, J. H. Mun, G. T. Hwang, J. M. Yoon, J. Y. Kim, J. M. Yun, Y. B. Yang, Y. Oh, J. Y. Lee, J. Shin, K. J. Soojin, U. K. Jaeup and O. K. Sang, *ACS Nano,* 2013, 7, 8899-8907.
29 W. Hwang, J. H. Choi, T. H. Kim, J. Sung, J. M. Myoung, D. G. Choi, B. H. Sohn, S. S. Lee, D. H. Kim and C. Park, *Chem. Mater.,* 2008, 20, 6041-6047.
30 S. Park, J. Y. Wang, B. Kim, W. Chen and T. P. Russell, *Macromolecules,* 2007, 40, 9059-9063.
31 A. Q. Wang, J. H. Liu, S. D. Lin, T. S. Lin and C. Y. Mou, *J. Catal.,* 2005, 233, 186-197.
32 M. Quintana, X. X. Ke, G. V. Tendeloo, M. Meneghetti, C. Bittencourt and M. Prato, *ACS Nano,* 2010, 4, 6105-6113.
33 T. Härtling, A. Seidenstucker, P. Olk, P. Alfred, P. Ziemann and L. M. Eng, *Nanotechnology,* 2010, 21, 145309.
34 Y. J. Liu, L. B. He, C. H. Xu and M. Han, *Chem. Commun.,* 2009, 6566-6568.
35 H.Ko, S. Singamaneni and V. V. Tsukruk, *Small,* 2008, 4, 1576-1599.
36 F. L. Yap, P. Thoniyot, S. Krishnan and S. Krishnamoorthy, *ACS Nano,* 2012, 6, 2056-2070.
37 L. Q. Lu, Y. Zheng, W. G. Qu, H. Q. Yu and A. W. Xu, J. *Mater. Chem.,* 2012, 22, 20986-20990.
38 M. J. Natan, *Faraday Discuss,* 2006,132, 321-328.

View Article Online
DOI: 10.1039/C6RA05225H

Table content of graphic